Geophys. J. R. astr. Soc. (1983) **73**, 523–532

Correction to: a thin viscous sheet model for continental deformation

Philip England *Harvard University, Department of Geological Sciences, 20 Oxford Street, Cambridge, MA 02138, USA*

Dan McKenzie *Department of Earth Sciences, University of Cambridge, Bullard Laboratories, Madingley Rise, Madingley Road, Cambridge CB3 0EZ*

Received 1982 November 1

Summary. The governing equation derived by England & McKenzie for the deformation of a thin viscous shell contains an error. We give the correct derivation here and correct those figures where the change makes a visible difference. The correct results differ quantitatively from those of England & McKenzie but their conclusions are not affected.

1 Formulation

We make the same assumptions as are discussed in sections 2.1 and 2.2 of England & McKenzie (1982), namely that the continental lithosphere can be approximated by a viscous shell whose thickness is small compared with the width of loads placed upon it and whose upper and lower surfaces are free of tractions. Under these conditions we may neglect vertical gradients of deviatoric stress and vertical variations of horizontal velocity components so that

$$\frac{\partial \tau_{ij}}{\partial z} = 0 \tag{1}$$

and

$$\dot{\epsilon}_{xz} = \dot{\epsilon}_{zx} = \dot{\epsilon}_{yz} = \dot{\epsilon}_{zy} = 0. \tag{2}$$

τ_{ij} are elements of the deviatoric stress tensor and $\dot{\epsilon}_{ij}$ elements of the strain rate tensor; x and y are horizontal coordinates and z is vertical *upwards*.

We further assume that the long-term and large strain rheology of the lithosphere is governed by the steady flow of one or more strength-controlling layers within the lithosphere whose rheology may be approximated by a flow law of the kind:

$$\tau_{ij} = B \dot{E}^{(1/n-1)} \dot{\epsilon}_{ij} \tag{3}$$

(England & McKenzie 1982, section 2 and appendix A). $\dot{E}$ is the second invariant of the strain rate tensor:

$$\dot{E} = (\dot{\epsilon}_{ij}\,\dot{\epsilon}_{ij})^{1/2} \tag{4}$$

with the convention of summation over repeated subscripts. The strain rate tensor is defined by:

$$\dot{\epsilon}_{ij} = \frac{1}{2}\left(\frac{\partial u_i}{\partial x_j} + \frac{\partial u_j}{\partial x_i}\right) \tag{5}$$

where u_i are velocity components. The incompressibility requirement and the above assumptions lead to an expression for $\dot{E}$ that involves only horizontal derivatives of velocity:

$$\dot{E} = \sqrt{2}\,(\dot{\epsilon}_{xx}^2 + \dot{\epsilon}_{yy}^2 + \dot{\epsilon}_{xy}^2 + \dot{\epsilon}_{xx}\,\dot{\epsilon}_{yy}). \tag{6}$$

In describing the flow of rocks at geological strain rates we may neglect momentum terms and the Navier-Stokes equation becomes

$$\frac{\partial \sigma_{ij}}{\partial x_j} = \rho g\, a_i \tag{7}$$

where $\mathbf{a} = (0, 0, 1)$ and we define the stress tensor, σ, by

$$\sigma_{ij} = \tau_{ij} + \frac{1}{3}\delta_{ij}\,\sigma_{kk} = \tau_{ij} - \delta_{ij}\,p. \tag{8}$$

Under the conditions we have assumed, the vertical component of equation (7) becomes

$$\frac{\partial \sigma_{zz}}{\partial z} = \rho g. \tag{9}$$

If we assume that the crustal thickness variations are in local isostatic equilibrium, the vertical stress has no horizontal gradient below the depth of compensation, and in particular we may choose σ_{zz} to be equal to $-P_0$ at the level $z = 0$, the base of the lithosphere. The normal stress on the upper surface of the lithosphere is zero; we shall assume that the top of lithosphere having no continental crust is at a level $z = L$; in isostatic equilibrium, the top of lithosphere having crustal thickness s is at $z = L + h$ where

$$h = s(1 - \rho_c/\rho_m) \tag{10}$$

where ρ_c and ρ_m are crust and mantle density, respectively. Equation (9) gives:

$$\sigma_{zz} = \tau_{zz} - p = g\int_0^z \rho dz + f(x, y) \tag{11}$$

and the boundary and isostasy conditions give

$$f(x, y) = -P_0 = -g\int_0^{L+h} \rho dz = -\rho_m L g. \tag{12}$$

As we have assumed that vertical gradients of the deviatoric stresses are negligible (equation 1) we may write the horizontal component of equation (7) as

$$\frac{\partial \tau_{\alpha\beta}}{\partial x_\beta} = \frac{\partial \bar{\tau}_{\alpha\beta}}{\partial x_\beta} = \frac{\partial \bar{p}}{\partial x_\alpha} \qquad \alpha, \beta = 1, 2 \tag{13}$$

where the bars denote vertical averages over the thickness of the lithosphere. The vertically averaged pressure may be calculated using equations (11) and (12)

$$\begin{aligned} p &= \tau_{zz} + P_0 - g \int_0^z \rho dz \\ \bar{p} &= \bar{\tau}_{zz} + P_0 - \frac{g}{L+h} \int_0^{L+h} dz' \int_0^{z'} \rho dz. \end{aligned} \tag{14}$$

With the assumption of isostatic equilibrium equation (14) becomes, after some algebra

$$\bar{p} = \bar{\tau}_{zz} + \frac{g\rho_c s^2}{2L}(1 - \rho_c/\rho_m) + \frac{g\rho_m L}{2} \tag{15}$$

for $h \ll L$. Substituting the expression for $\bar{\tau}_{ij}$ and $\bar{p}$ from equations (3) and (15) gives:

$$\frac{\partial}{\partial x_\beta}\left(B\dot{E}^{(1/n-1)}\dot{\epsilon}_{\alpha\beta}\right) + \frac{\partial}{\partial x_\alpha}\left[B\dot{E}^{(1/n-1)}(\dot{\epsilon}_{xx} + \dot{\epsilon}_{yy})\right] = \frac{g\rho_c s(1-\rho_c/\rho_m)}{L}\frac{\partial s}{\partial x_\alpha}. \tag{16}$$

Using the same non-dimensionalization as England & McKenzie (1982):

$$(x', s') = (x, s)/L; \qquad u' = u/u_0; \qquad t' = t\,u_0/L$$

$$Ar = \frac{gL\rho_c(1-\rho_c/\rho_m)}{B(u_0/L)^{1/n}}$$

and dropping primes, equation (16) may be written

$$\nabla^2 \mathbf{u} = -3\nabla(\nabla\cdot\mathbf{u}) + 2(1-1/n)\dot{E}^{-1}[\nabla\dot{E}\cdot\dot{\boldsymbol{\epsilon}} + (\nabla\cdot\mathbf{u})\nabla\dot{E}] + 2Ar\dot{E}^{(1-1/n)}s\nabla s \tag{17}$$

where $\dot{\boldsymbol{\epsilon}}$ is the horizontal strain rate tensor whose elements are $\dot{\epsilon}_{\alpha\beta}$ and all operators refer to horizontal derivatives only. This replaces equation (16) of England & McKenzie. The means of solution area, *mutatis mutandis,* those of appendix B of England & McKenzie.

2 Results

The term in $\nabla(\tau_{zz})$ (equation 16) which was missing from the formulation of England & McKenzie (1982) is a pressure gradient acting away from the region of most intense compression. Consequently the solutions shown here exhibit a more diffuse deformation than those of England & McKenzie. Figs 1–10 show the correct solutions, corresponding to figs 2–7 and 9–12 of England & McKenzie. The greatest difference is seen at low Argand number and plots of velocity, principal stress principal strain rate are included for $Ar = 0$, $n = 1$, 3 and 5 (Figs 1–3); for non-zero Argand number, these plots do not show visible differences from the incorrect ones. Figs 4–6 show the crustal thickness as a function of time for these conditions.

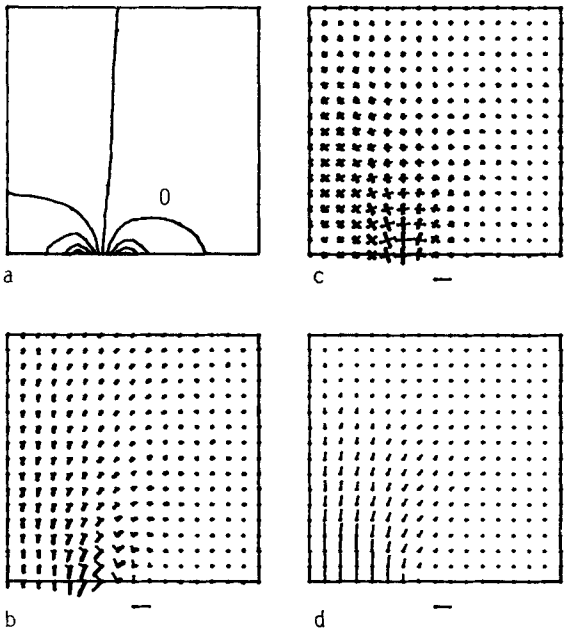

Figure 1. Replaces fig. 2 of England & McKenzie (1982). In this and all subsequent figures, the velocity, differential stress and strain rates, when displayed, are shown at spacings of $2L$ (that is at every second point in x and y for a 32×32 grid). Contours are drawn by a standard contouring routine that uses values from all the mesh points. This figure illustrates the velocity, strain rate and differential stress fields for a Newtonian fluid subject to the boundary conditions shown in fig. 1 of England & McKenzie (1982) with $Ar = 0$. (a) Isotropic strain rate field [contours of the instantaneous rate of thickening or thinning: $-(\dot{\epsilon}_{xx} + \dot{\epsilon}_{yy})$] for the flow field. The contours are from -6×10^{-16} to $10^{-15}\,s^{-1}$ in steps of $2 \times 10^{-16}\,s^{-1}$. (b) Directions and magnitudes of the principal horizonal deviatoric stresses produced by the flow; the bar below the figure shows the size of the symbol for the stress with the greatest magnitude. When $Ar = 0$ the absolute value of the stress is arbitrary, and Figs 1, 2 and 3 depict the relative magnitudes of the principal stresses. The origins of the symbols lie on the mesh points; thick lines indicate negative stress (compression) and thin lines indicate positive stress (tension). (c) Directions and magnitudes of principal shear strain rates for the flow; the bar below the figure shows the size of the symbol for the maximum strain rate ($9.1 \times 10^{-16}\,s^{-1}$). The centres of the symbols lie on the mesh points; thick lines correspond to dextral shear, and the thin lines to sinistral shear. (d) Velocity vectors for the flow at individual mesh points, the origins for the vectors being at these points. The maximum velocity, shown by the bar below the figure is 50 mm yr^{-1}.

With non-zero Argand number, the lower compressional strain rates relative to those of England & McKenzie mean that it takes longer for crustal thickness to build up, but the same behaviour is exhibited as in the original figures: for a given Argand number there is an effective limit to the crustal thickness that a given flow can support; here it is reached after 32 Myr in most cases whereas it is reached earlier in the incorrect formulation, so plots of crustal thickness and $\dot{\epsilon}_{zz}$ are shown at intervals up to 40 Myr for $n = 3$, $Ar = 1, 3, 10$ and 30. The maximum crustal thickness reached in these cases is 120 km ($Ar = 1$), 85 km ($Ar = 3$), 60 km ($Ar = 10$) and 50 km ($Ar = 30$) at 40 Myr (Figs 7–10), compared to 120, 80, 55 and 45 km, respectively, after 32 Myr (England & McKenzie, figs 9–12).

The other main difference lies in the decreased prominence of regions of net extension; these only occur for Argand numbers of 3–10 (Figs 8 and 9), but once the maximum supportable crustal thickness has been attained there is still a broad region where $\dot{\epsilon}_{zz}$ is low

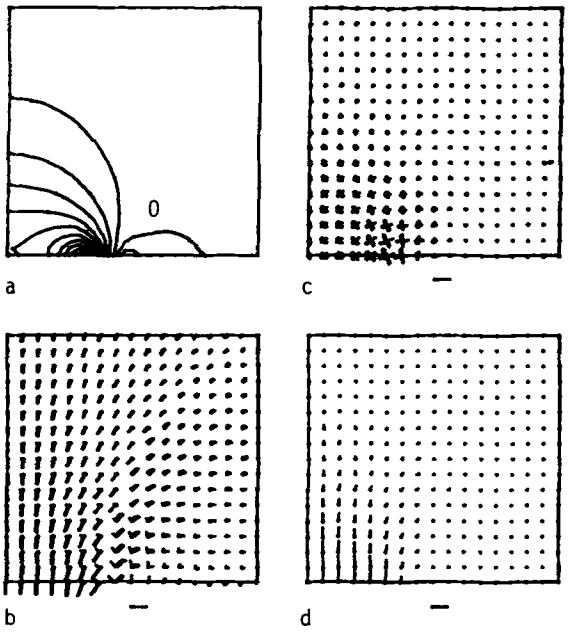

Figure 2. Replaces fig. 3 of England & McKenzie (1982). As for Fig. 1, except that the solutions are for a non-Newtonian power-law fluid with $n = 3$ and $Ar = 0$. (a) The strain rate contours are $-2\times10^{-16}\,s^{-1}$ $(2\times10^{-16}\,s^{-1})$ $2\times10^{-15}\,s^{-1}$. (c) The maximum principal shear strain rate is $1.3\times10^{-15}\,s^{-1}$.

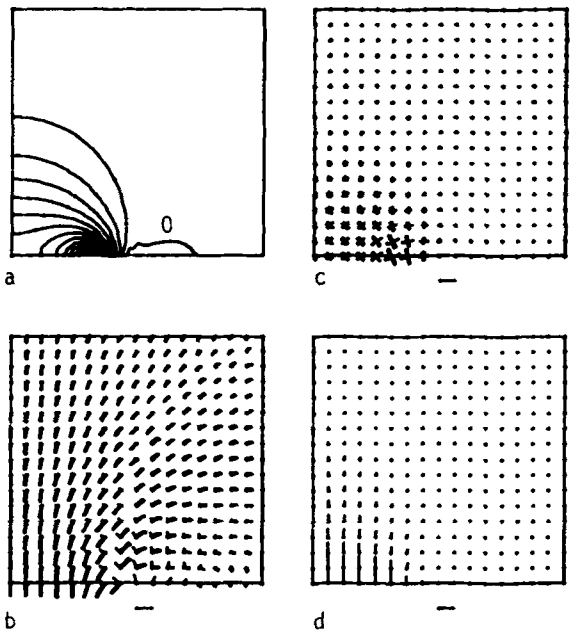

Figure 3. Replaces fig. 4 of England & McKenzie (1982). As Fig. 2 except that n is 5 and Ar is zero. (a) The strain rate contours are 0 $(2\times10^{-16}\,s^{-1})$ $2.4\times10^{-15}\,s^{-1}$. (c) The maximum principal shear strain rate is $1.5\times10^{-15}\,s^{-1}$.

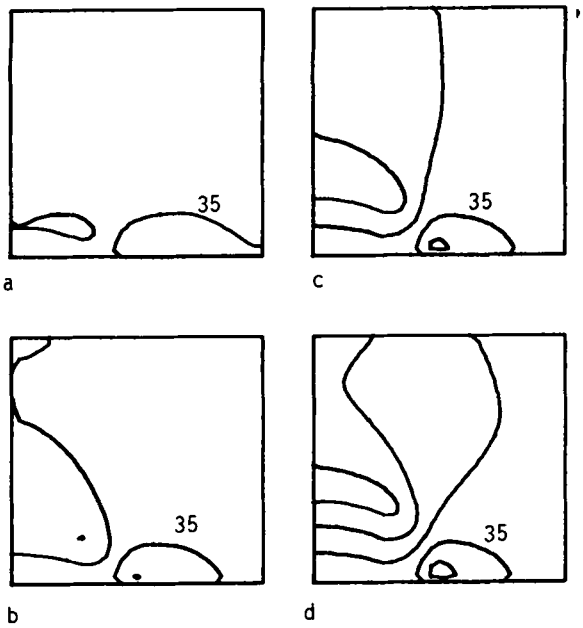

Figure 4. Replaces fig. 5 of England & McKenzie (1982). Plots of crustal thickness as a function of time for the flow field of fig. 1. Contours are at intervals of 5 km thickness; the thickness of crust entering over the influx boundary is 35 km. The 35 km contours are labelled. (a) Time is 7.9 Myr; contours are from 35 km in steps of 5 km to 40 km. (b) Time is 15.7 Myr; crustal thickness 30 (5) 45 km. (c) Time is 23.6 Myr; crustal thickness 30 (5) 45 km. (d) Time is 31.7 Myr; crustal thickness 30 (5) 50 km.

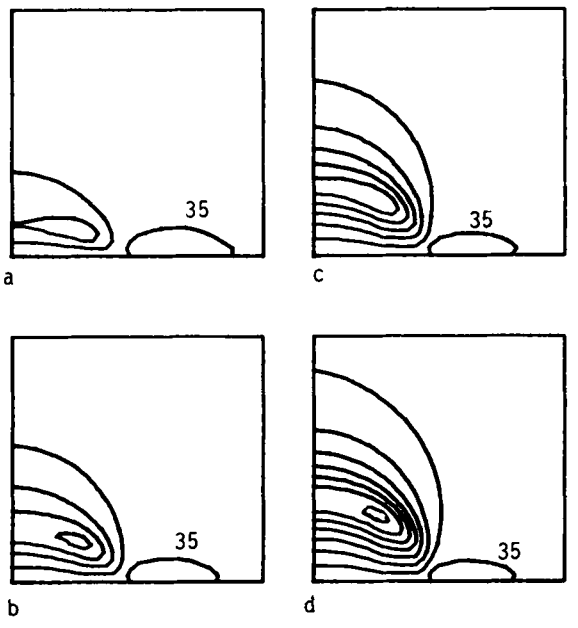

Figure 5. Plots of crustal thickness as a function of time for the flow fields of Fig. 3. As Fig. 4. (a) Time is 7.9 Myr; crustal thickness contours are 35 (5) 45 km. (b) Time is 15.8 Myr; crustal thickness 35 (5) 55 km. (c) Time is 23.8 Myr; crustal thickness 35 (5) 60 km. (d) Time is 31.7 Myr; crustal thickness 35 (5) 70 km.

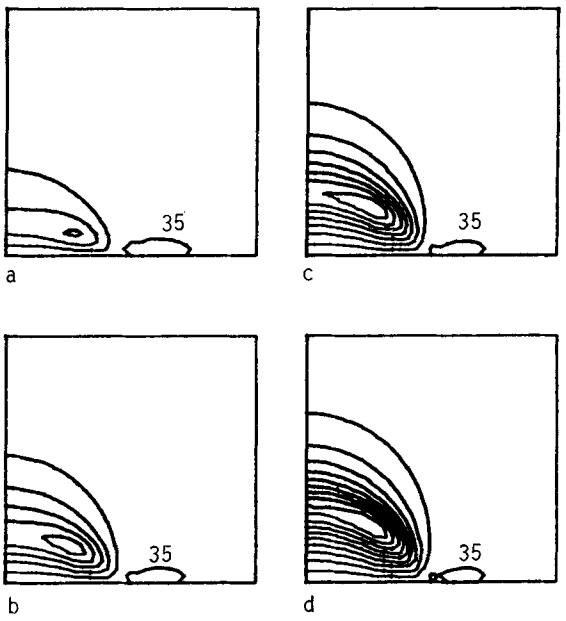

Figure 6. Plots of crustal thickness as a function of time for the flow fields of Fig. 4. As Fig. 5. (a) Time is 7.9 Myr; crustal thickness contours are 35 (5) 50 km. (b) Time is 15.8 Myr; crustal thickness 35 (5) 60 km. (c) Time is 23.8 Myr; crustal thickness 35 (5) 70 km. (d) Time is 31.8 Myr; crustal thickness 35 (5) 80 km.

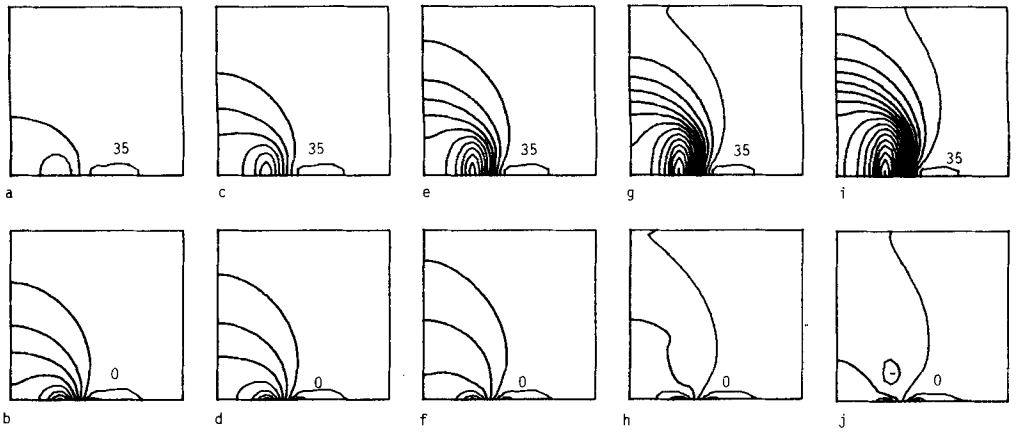

Figure 7. Replaces fig. 9 of England & McKenzie (1982). Contours of crustal thickness and isotropic strain rate for the boundary conditions of England & McKenzie (1982, fig. 1), with $n = 3, Ar = 1$. The crustal thickness is contoured at 5 km intervals and the strain rate at intervals of $2 \times 10^{-16}\,s^{-1}$. In this and subsequent figures, maxima and minima in the contoured variables are indicated by addition and subtraction signs, when necessary. (a) Time is 7.9 Myr; crustal thickness contours are from 35 km in steps of 5 km to 45 km. (b) Time is 7.9 Myr; isotropic strain rate contours are from $-2 \times 10^{-16}\,s^{-1}$ in steps of $2 \times 10^{-16}\,s^{-1}$ to $1.6 \times 10^{-15}\,s^{-1}$. (c) Time is 15.8 Myr; crustal thickness 35 (5) 65 km. (d) Time is 15.8 Myr; isotropic strain rate -2×10^{-16} (2×10^{-16}) $1.4 \times 10^{-15}\,s^{-1}$. (e) Time is 23.7 Myr; crustal thickness 35 (5) 85 km. (f) Time is 23.7 Myr; isotropic strain rate -2×10^{-16} (2×10^{-16}) $1.2 \times 10^{-15}\,s^{-1}$. (g) Time is 31.6 Myr; crustal thickness 35 (5) 105 km. (h) Time is 31.6 Myr; isotropic strain rate -4×10^{-16} (2×10^{-16}) $10^{-15}\,s^{-1}$. (i) Time is 39.4 Myr; crustal thickness 35 (5) 120 km. (j) Time is 39.4 Myr; isotropic strain rate -4×10^{-16} (2×10^{-16}) $8 \times 10^{-16}\,s^{-1}$.

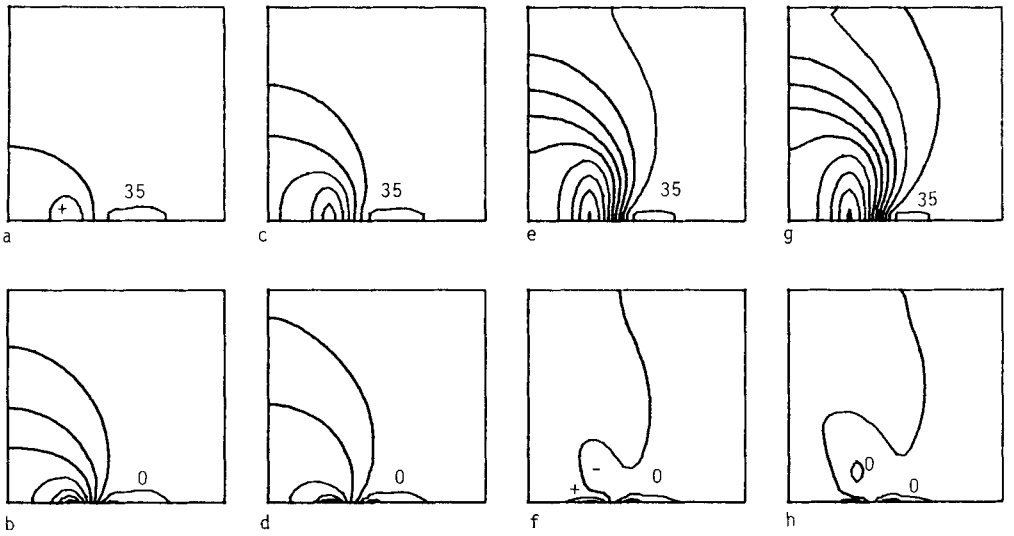

Figure 8. Replaces fig. 10 of England & McKenzie (1982). As Fig. 7 with $n = 3$ and $Ar = 3$. (a) Time is 7.9 Myr; crustal thickness contours are from 35 km in steps of 5 km to 45 km. (b) Time is 7.9 Myr; isotropic strain rate contours are from $-2\times10^{-16}\,s^{-1}$ in steps of $2\times10^{-16}\,s^{-1}$ to $1.6\times10^{-15}\,s^{-1}$. (c) Time is 15.8 Myr; crustal thickness 35 (5) 60 km. (d) Time is 15.8 Myr; isotropic strain rate -2×10^{-16} (2×10^{-16}) $1.2\times10^{-15}\,s^{-1}$. (e) Time is 31.4 Myr; crustal thickness 35 (5) 80 km. (f) Time is 31.4 Myr; isotropic strain rate -4×10^{-16} (2×10^{-16}) $8\times10^{-16}\,s^{-1}$. (g) Time is 39.2 Myr; crustal thickness 35 (5) 85 km. (h) Time is 39.2 Myr; isotropic strain rate -4×10^{-16} (2×10^{-16}) $6\times10^{-16}\,s^{-1}$.

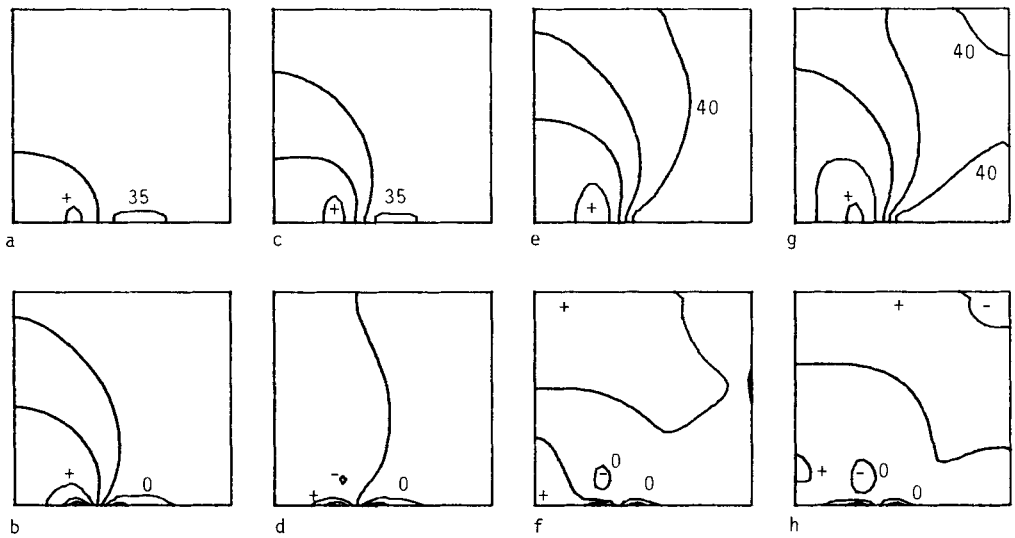

Figure 9. Replaces fig. 11 of England & McKenzie (1982). As Fig. 7, with $n = 3$ and $Ar = 10$. (a) Time is 7.9 Myr; crustal thickness contours are from 35 km in steps of 5 km to 45 km. (b) Time is 7.9 Myr; isotropic strain rate contours are from $-2\times10^{-16}\,s^{-1}$ in steps of $2\times10^{-16}\,s^{-1}$ to $1.2\times10^{-15}\,s^{-1}$. (c) Time is 15.7 Myr; crustal thickness 35 (5) 50 km. (d) Time is 15.8 Myr; isotropic strain rate -4×10^{-16} (2×10^{-16}) $8\times10^{-16}\,s^{-1}$. (e) Time is 31.2 Myr; crustal thickness 40 (5) 55 km. (f) Time is 31.2 Myr; isotropic strain rate -4×10^{-16} (2×10^{-16}) $6\times10^{-16}\,s^{-1}$. (g) Time is 38.0 Myr; crustal thickness 40 (5) 60 km. (h) Time is 38.9 Myr; isotropic strain rate -2×10^{-16} (2×10^{-16}) $6\times10^{-16}\,s^{-1}$.

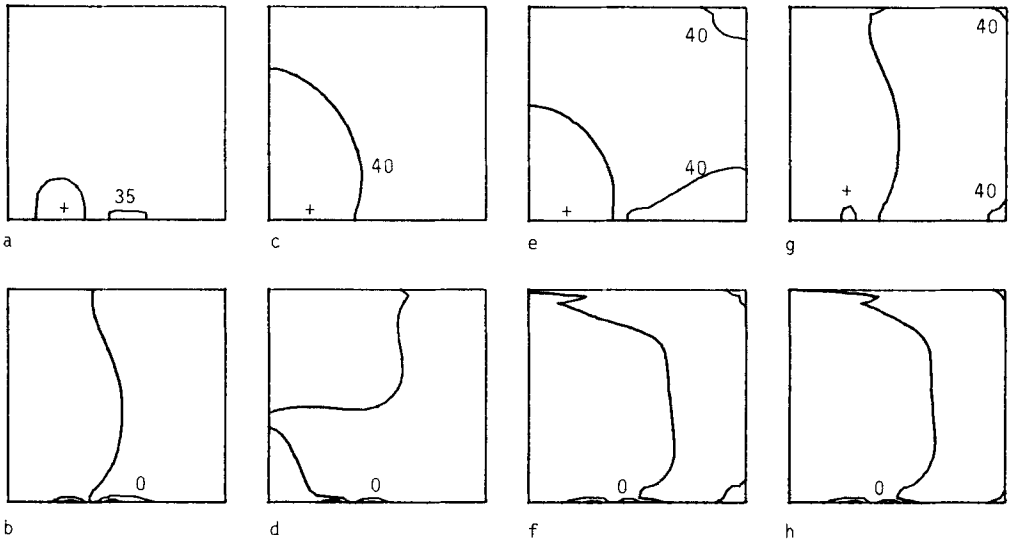

Figure 10. Replaces fig. 12 of England & McKenzie (1982). As Fig. 7, with $n = 3$, $Ar = 30$. (a) Time is 7.9 Myr; crustal thickness contours are from 35 km in steps of 5 km to 40 km. (b) Time is 7.9 Myr; isotropic strain rate contours are from $-4 \times 10^{-16}\,s^{-1}$ in steps of $2 \times 10^{-16}\,s^{-1}$ to $8 \times 10^{-16}\,s^{-1}$. (c) Time is 15.6 Myr; crustal thickness contour of 40 km is shown. (d) Time is 15.6 Myr; isotropic strain rate -2×10^{-16} (2×10^{-16}) $6 \times 10^{-16}\,s^{-1}$. (e) Time is 31.0 Myr; crustal thickness 40 (5) 45 km. This corresponds closely to fig. 12(e) of England & McKenzie (1982) where the 40 km contour is incorrectly labelled as a 35 km contour. (f) Time is 31.0 Myr; isotropic strain rate -2×10^{-16} (2×10^{-16}) $6 \times 10^{-16}\,s^{-1}$. (g) Time is 38.7 Myr; crustal thickness 40 (5) 50 km. (h) Time is 38.7 Myr; isotropic strain rate -2×10^{-16} (2×10^{-16}) $6 \times 10^{-16}\,s^{-1}$.

(10–20 per cent of the original maximum value) that covers much of the area of thickest crust (Figs 7–10). It may also be seen that one principal strain rate in this region is extensional, comparable in magnitude to the compressional one, and is orientated approximately parallel to the influx boundary (England & McKenzie, fig. 13, which is not visibly different from the correct figure).

3 Conclusion

The principal effect of the incorrect formulation of England & McKenzie was to diminish the length scale of the deformation and so, relative to the correct formulation, to produce more intense deformation near the influx boundary and less intense deformation away from this boundary. Because of this, the magnitudes of the crustal thickness and strain rates shown in Figs 1–10 of this paper differ from those in the original paper; these changes are not sufficient to affect the general discussion of their results made by England & McKenzie and, in particular, England & McKenzie's conclusions still hold:

(a) Over a wide range of rheological parameters, the thin viscous sheet model for continental deformation predicts that, in a continental collision such as that of India and Asia, thickening of the continental crust will occur over areas of linear dimension comparable with the width of the indenting continent. The broad zone of elevated and thickened crust extending more than 1500 km north of the Himalaya is consistent with such a view of continental deformation.

(b) For a fixed geometry of collision, the deformation of such a sheet is governed by two parameters: n, the exponent in the power-law rheology, and Ar, the Argand number, which is a measure of the tendency of the lithosphere to strain in response to buoyancy forces arising from crustal thickness contrasts. For any $Ar > 0$, there is an upper limit to the crustal thickness that can be supported by compressional boundary conditions. Initially deformation consists of compression localized round the influx boundary, but as the buoyancy forces due to crustal thickness contrasts increase, the influx of material can no longer be accommodated by continued thickening near the influx boundary; instead, the deformation takes the form of less intense compression spread over a wider area (Figs 7–10). Once this stage is reached, the principal deviatoric stresses in the region of thickest crust are compressive, approximately normal to the influx boundary, and extensional, approximately parallel to it. These stresses are close in magnitude, so the net rate of thickening is small in this region and when the Argand number is 3 or greater there is net extension in this region (England & McKenzie, fig. 13 and Figs 7–10). This transition in deformation style from intense compressive strain in the early phases to almost-plane-strain once the maximum supportable crustal thickness is reached is a distinctive feature of the strain history of a thin viscous sheet with non-zero Argand number.

Reference

England, P. C. & McKenzie, D. P., 1982. A thin viscous sheet model for continental deformation, *Geophys. J. R. astr. Soc.*, **70**, 295–321.